Photonic Newton's Cradle for Remote Energy Transport

Zhen Feng,[1,2] Zhen-Wei Gao,[1,3] Lian-Ao Wu,[4,5] Hao Tang,[1,2] Ke Sun,[1,3] Cheng-Qiu Hu,[1,2] Yao Wang,[1,2,6] Zhan-Ming Li,[1,2] Xiao-Wei Wang,[1] Yuan Chen,[1,2,6] En-Ze Zhang,[1] Zhi-Qiang Jiao,[1,2] Xiao-Yun Xu,[1,2] Jun Gao,[1,2,6] Ai-Lin Yang,[1,2] and Xian-Min Jin[1,2,*]

[1] *School of Physics and Astronomy, Shanghai Jiao Tong University, Shanghai 200240, China*

[2] *Synergetic Innovation Center of Quantum Information and Quantum Physics,University of Science and Technology of China, Hefei, Anhui 230026, China*

[3] *Zhiyuan Innovative Research Center, Shanghai Jiao Tong University, Shanghai 200240, China*

[4] *Ikerbasque, Basque Foundation for Science, Bilbao 48011, Spain*

[5] *Department of Theoretical Physics and History of Science, University of Basque Country, Bilbao 48080, Spain*

[6] *Institute for Quantum Science and Engineering and Department of Physics, Southern University of Science and Technology, Shenzhen 518055, China*

(Received 1 November 2018; revised manuscript received 4 February 2019; published 3 April 2019)

Energy transport is of central importance in understanding a wide variety of transitions of physical states in nature. Recently, the coherence and noise have been identified for their existence and key roles in energy-transport processes, for instance, in a photosynthesis complex, DNA, and odor sensing etc., of which one may have to reveal the inner mechanics in the quantum regime. Here we present an analog of Newton's cradle by manipulating a boundary-controlled chain on a photonic chip. Long-range interactions can be mediated by a long chain composed of 21 strongly coupled sites, where single-photon excitations are transferred between two remote sites via simultaneous control of intersite weak and strong couplings. We observe a high retrieval efficiency in both uniform and defect-doped chain structures. Our results may offer a flexible approach to Hamiltonian engineering beyond geometric limitation, enabling the design and construction of quantum simulators on demand.

DOI: 10.1103/PhysRevApplied.11.044009

I. INTRODUCTION

Energy transport, unveiling the evolution of physical states and the nature of particle interactions, has long been discussed. A quantum particle that can also be represented as a wave function possesses quantum-inherent interference and has a superposition of many locations or paths, and quantum-involved energy transport in the quantum regime is stepping into fascinating frontiers [1–6].

A ballistic spread has been performed when a quantum particle propagates in ideally ordered lattices [7]. However, the energy mismatch between sites in a practical system Hamiltonian may lead to localization [8,9], and the interaction with environment may result in decoherence [10]. For instance, unexpected accumulated phases or amplitudes may cause the suppression of broadening wave package [9,11].

A chain, linearly arranged sites between nearest-coupled neighbors, has been considered for energy transport between information terminals at a distance, which is crucial in constructing large-scale quantum-information networks. Two types of chains, fully engineered chain and boundary-controlled chain, have been proposed to realize energy transport. The fully engineered chain with N sites requires an accurate coupling modulation of $\sqrt{i(N-i)}$ on the structural configuration of the i_{th} site, and a perfect spatial mirror image of the injection after a half period to perform perfect retrieval of photons [12–14]. The transfer efficiency is highly dependent on the manufacturing precision associated with both external and internal regularity. The high parameter sensitivity demanded in theory and unavoidable imperfections in practice make the chain hard to scale up.

In contrast, a boundary-controlled chain as a new model was proposed and it required a minimal control while possessing a well-behaved robustness [15]. A series of linearly arranged and strongly coupled sites form a chain to bridge two remote sites, denoted as sending and receiving sites. The two sites are coupled to the end of the chain with a very weak coupling [16,17]. A quantum particle injected into the sending site can propagate through the boundary-controlled chain and go back and forth to the receiving site, with a fashion of energy transport like Newton's cradle. A straightforward model (with only two

*xianmin.jin@sjtu.edu.cn

parameters of strong and weak couplings) and its intrinsic robustness make the protocol of boundary-controlled chain a promising candidate for energy transport. The boundary-controlled chain models were widely investigated and have been applied to different physical systems [18–26], which, however, have not been experimentally demonstrated yet.

II. RESULTS

A. Photonic analog of Newton's cradle

In this paper, we prototype waveguides as the sites of the chain by using the femtosecond laser direct-writing technique [27–30] and successfully map the boundary-controlled chain onto a photonic chip (see Appendix A). In this manner, the propagation length of photons in waveguides on chip is equivalent to the evolution time in the chain, due to the constant speed of photons within the chip [30]. As shown in Fig. 1, a photon is launched on the left sending site, weakly coupled to a head-tail strongly coupled chain, then also weakly coupled to the right receiving site. Such a boundary-controlled chain can transfer single photons faithfully and therefore can serve like a photonic Newton's cradle for enabling interactions between remote sites in a quantum network.

The Hamiltonian is composed of strong couplings $J_n = J, (n = 2, 3, \ldots, N-2)$ and weak couplings $J_1 = J_{N-1} = \alpha J (\alpha \ll 1)$. The parameter α reflects the differential strength between strong and weak couplings. A single-photon state $|\Psi_0\rangle$ is injected in the sending site. Initial state of the N-body system, which can be presented as $|\Phi(t=0)\rangle = |\Psi_0\rangle \otimes |00\ldots0\rangle$ evolves with the Hamiltonian:

$$H = J_1 a_1^\dagger a_2 + J_{N-1} a_{N-1}^\dagger a_N + \sum_{i=2}^{N-2} J a_i^\dagger a_{i+1} + \text{c.c.} \quad (1)$$

Here we employ a coupled mode approach to experimentally characterizing the coupling strength between two waveguides [27].

The state of the system at a given time t is $|\Phi(t)\rangle = e^{-iHt/\hbar}|\Phi(t=0)\rangle$. Given the parameters N and α, we have the highest efficiency $\eta = 1 - O(\alpha^2 N)$ in the optimal receiving time

$$\tau = \frac{\pi\sqrt{N-2}}{2(\alpha J)}, \quad (2)$$

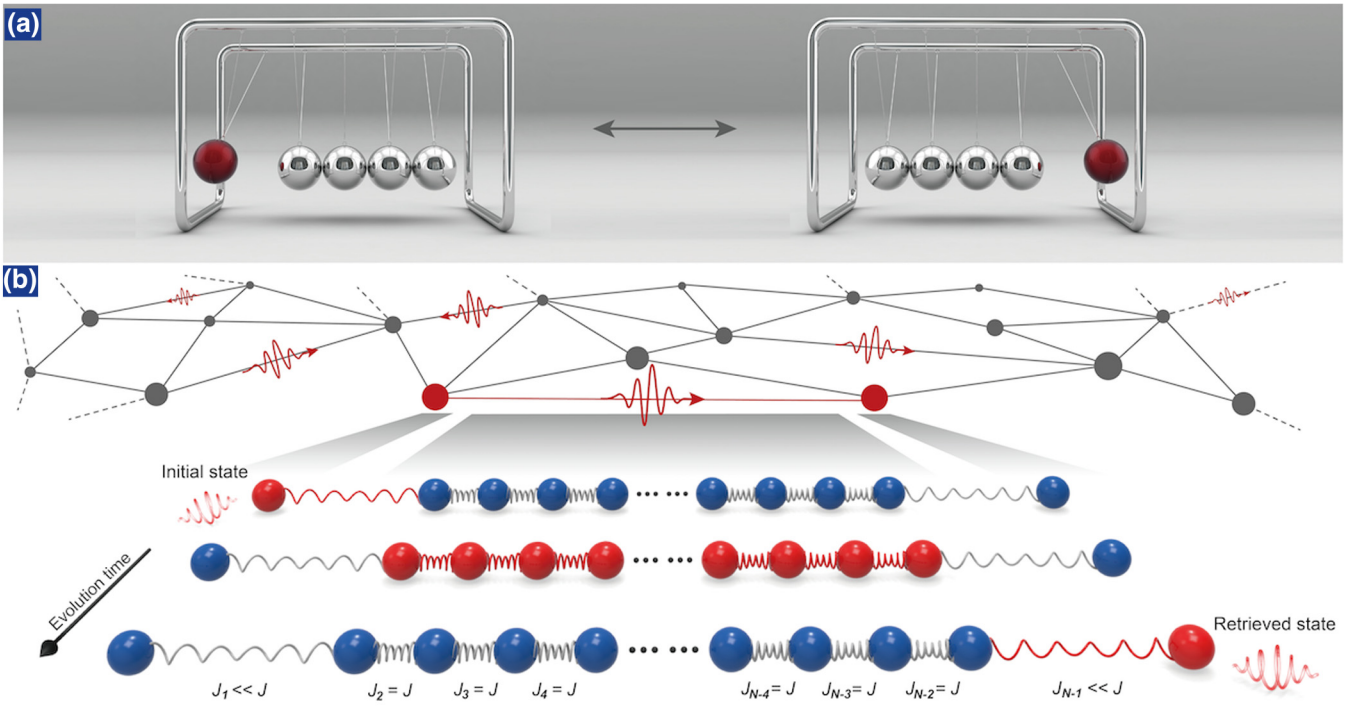

FIG. 1. Energy transport in Newton's cradle and its analog in a photonic system. (a) Energy exchange and interaction mechanics in Newton's cradle. The energy can be transfered from the leftmost ball to the rightmost one mediated by a chain of balls, in effect, which is equivalent to the scenario that the two balls interact each other directly. (b) Energy transport between remote sites in a quantum network. The photonic analog of Newton's cradle is realized by a boundary-controlled chain. The chain consists of weak coupling αJ in two ends and a chain of strongly coupling J in the middle, which gives an equivalent coupling for the two remote sites. The obtained long-range interaction could enable a faithful transfer of quantum states. An initial state can be transfered to the remote receiving site faithfully and therefore can serve like a photonic Newton's cradle for enabling interactions between remote sites in a quantum network.

where the capital O notation is made use of keeping track of the leading term that dominates scaling [31]. In fact, the optimal receiving time τ and transfer efficiency η are a trade-off. A high efficiency is at the cost of a weak coupling ($\alpha < 1/\sqrt{N}$) and a faithful transfer can be obtained asymptotically with α nearly vanishing [32].

B. Implementation of photonic Newton's cradle

Our aim of energy transport is to transfer photonic states, excited at the first site through the chain and retrieved at the remotely separated receiving site N with a high efficiency η. Efficiency peaks when evolution time t reaches the optimal τ. In our experiment, we set the parameter $\alpha = 0.12 < 1/\sqrt{23}$ and design the boundary-controlled photonic lattices as shown in Fig. 2(a). According to the characterized coupling strength with the injection of coherent light at 810 nm [see Fig. 2(b) and Appendix B], the strong coupling strength J is chosen at 1.526 mm^{-1} in a uniform site pitch of 5 μm between 21 nearest-neighbor sites. The boundary coupling strength is chosen at 0.189 mm^{-1} in the site pitch of 16 μm to the ends of the chain.

The chain is able to transfer energy between two remote sites with the same fashion of energy exchange and interaction mechanics of Newton's cradle:

$$H = J_{\text{eff}} a_1^{\dagger} a_N + \text{c.c.}, \tag{3}$$

where effective coupling coefficient J_{eff} is derived by $\alpha J/\sqrt{N-1}$ and is also shown in Fig. 2(b). Previous works deduce the practical meaning of the effective coupling coefficient J_{eff} only from a theoretical view and here we perform a direct experimental observation. The effective coupling coefficient is only related to the weak coupling

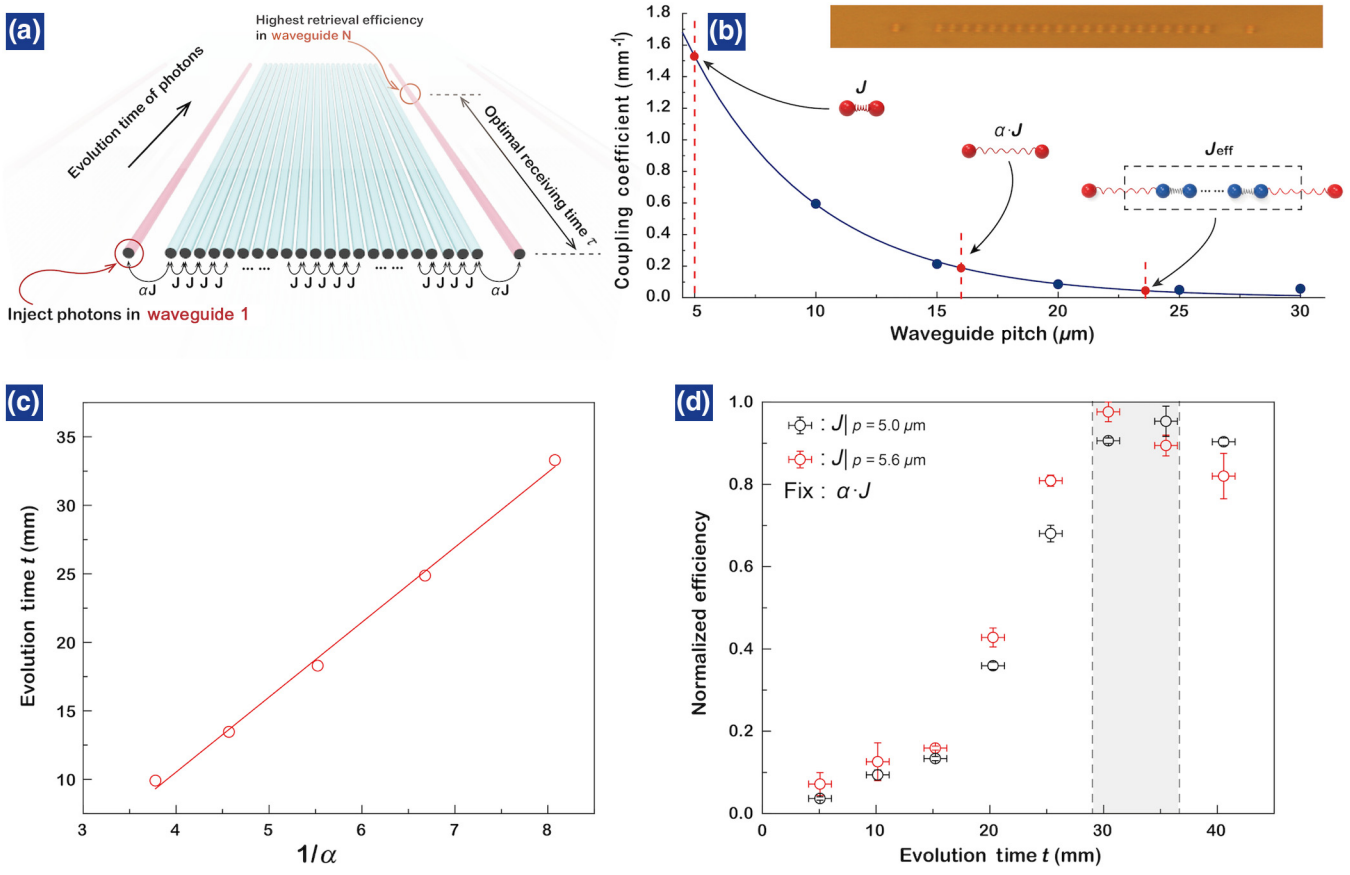

FIG. 2. Design and implementation of the boundary-controlled chain. (a) Schematic graph of the 3D photonic Newton's cradle waveguide system. (b) Characterized coupling coefficients and their exponential dependence on the waveguide pitches [27]. An effective coupling coefficient can be designed by choosing appropriate αJ and J, respectively. Blue dots show experimental measurements. Red dashed lines and spots mark the parameters mainly adopted in this work. The inset is the cross section of a set of waveguide arrays with designed pitches. (c) The linear relation, as indicated in Eq. (2), is observed by scanning $1/\alpha$ while keeping J constant. Here, the evolution time t, in units of mm, is defined by the evolution length of photons in the waveguide array. (d) The robustness of the model is demonstrated by showing the insensitivity of the evolution time on the strong coupling J. The small shift can be attributed to the unavoidable experimental imperfections and the fact that the condition $\alpha \ll 1$ is not strictly satisfied.

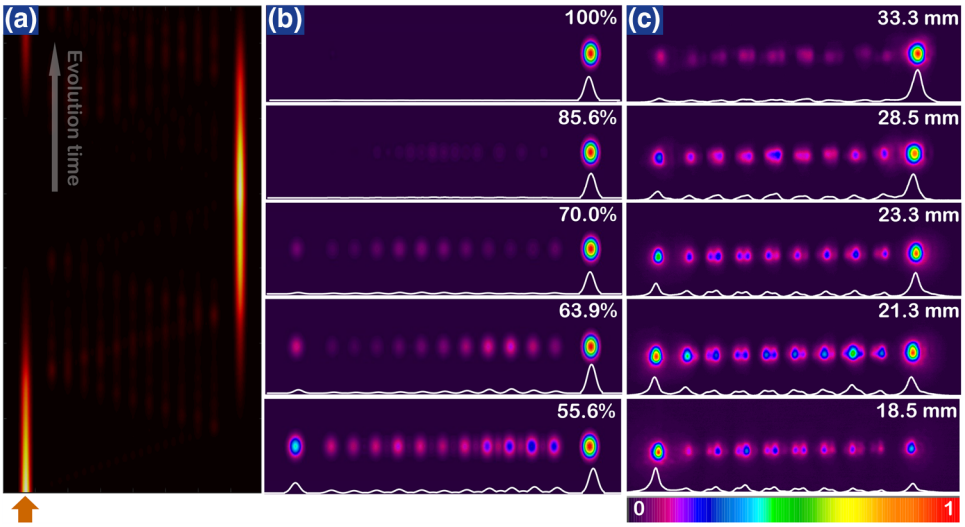

FIG. 3. Theoretical and experimental results of time evolution and transverse intensity distribution. (a) Numerical results of light propagation in the system with two boundary coupling sites and 21 strongly coupling sites. (b),(c) Theoretical and experimental results of the transverse intensity distribution in five different propagation lengths or evolution times (18.5, 21.3, 23.3, 28.5, and 33.3 mm).

coefficient αJ, and can be obtained by measuring the optimal receiving time τ according to Eq. (2). We experimentally keep J constant and tune αJ by setting five different weak coupling separations from 12 to 15 μm spacing 1 μm as shown in Fig. 2(c). With linear fitting we obtain a slope of 5.470, which indicates that the experimentally obtained strong coupling strength J is up to 1.316 mm^{-1}.

For a wide range where the boundary-controlled condition is satisfied, the whole system behaves like a direct interaction between two remote sites, just like Newton's cradle, i.e., without considering the chain at the middle. We fix the weak coupling coefficient αJ and adjust finely the site pitch from 5 to 5.6 μm to acquire the strong coupling strength J from $J|_{p=5}$ to $J|_{p=5.6}$. We measure the transverse intensity distribution while scanning the propagation length or evolution time t. The shading period in Fig. 2(d) shows that a trend fitting of experimental data gives the same τ. Our measurement supports the theory that the optimal receiving time is independent of the strong coupling strength and mainly relies on the weak coupling strength.

We visualize the time evolution of coherent light in the system by showing the imaged transverse intensity distribution at five different evolution times (see Fig. 3). Experimentally this is implemented by fabricating five such samples. The probability of the excitation at the i_{th} site is given by $p_i(t) = |\langle i|\Phi(t)\rangle|^2$, where $p_1(0) = 1$. An optimal receiving time for faithful transfer can be found at the evolution time of 33.3 mm. The direct observed optimal receiving time slightly deviates away from the value of 40.25 mm predicted with the characterized coupling strength, which is due to the fact that the coupling strength does not rigorously follow the exponential relation to the propagation length in the very near coupling region. In addition, the next-nearest-neighbor coupling, fabrication imperfection, and even artificially introduced defects may also affect the real transfer performance.

C. Quantum correlation verification

Besides fundamental interest on the analog to Newton's cradle and the offered alternative approach for energy transport, the demonstrated boundary-controlled chain also provides an elegant way to mediate long-range interactions on a photonic chip for quantum applications. To confirm its compatibility to quantum technologies, we inject heralded single photons instead of coherent light and measure the intensity distribution with single-photon imaging technique [see Fig. 4(a) and Appendix C]. The injected photon from a single arm of our photon pair is actually a thermal light. With the trigger of a successful registration of the other photon, we are able to measure the output intensity distribution of genuine heralded single photons. For single-party injection, there is no difference on the optimal receiving time for coherent light, thermal light, and single photons [see Fig. 4(b) and 4(c)].

In order to verify whether quantum correlation can be preserved in the evolution, we employ the Hanbury-Brown-Twiss interferometer shown in Fig. 4(a) to measure photon statistics of the output states. The anticorrelation function

$$g^{(2)}(0) = \frac{p_1 p_{123}}{p_{12} p_{13}} \tag{4}$$

tends to 0 for an ideally prepared single-photon state and tends to larger than 1 for classical light [33]. Here, p_1 means the probability of a count in detector 1, and p_{12}, p_{13}, and p_{123} represent the probabilities of simultaneous counts in those detectors. We observe an anticorrelation up to 0.0089 ± 0.0019, which suggests that single-photon property can be well preserved through the single-photon Newton's cradle.

D. Defect-induced enhancement of efficiency

Recently, the coherence and noise have been identified for their existence and key roles in energy-transport

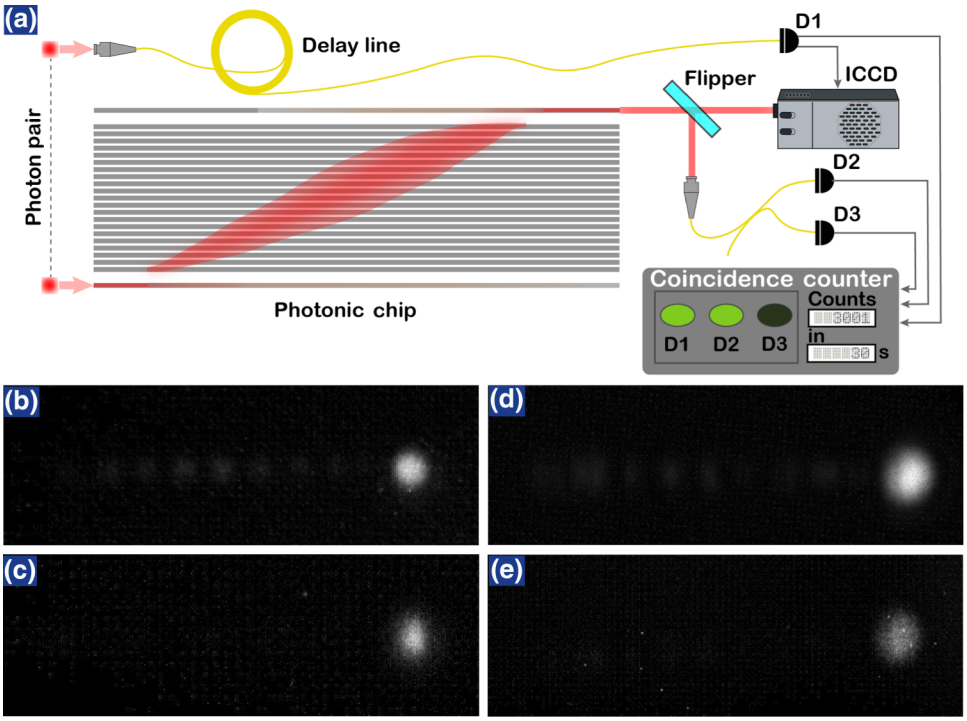

FIG. 4. Single-photon Newton's cradle. (a) Experimental setup. A flipper mirror allows the detection system to be switched from direct single-photon imaging to Hanbury-Brown-Twiss interference. (b),(c) Measured output intensity distribution of thermal light and heralded single photons for a standard boundary-controlled chain. (d),(e) Measured output intensity distribution of thermal light and heralded single photons with an additional island site on the top middle of the chain.

processes, for instance, in a photosynthesis complex [3,4], DNA [5], and odor sensing [6] etc., in which we may have to explain the inner mechanics in the quantum regime. Counterintuitively, early work suggested that the noise and decoherence may have a positive influence on quantum processes [4,10,23,24,34,35]. Meanwhile, theoretical investigation has also shown that the boundary-controlled chain may be a fault-tolerant system [17]. We construct a nonideal scenario by adding an island site next to the central site with the same separation as other strong coupled sites. The newly added island site can be considered as noise, defect, or environment to the original boundary-controlled chain. The imaged output intensity distributions with thermal light and heralded single photons are shown in Figs. 4(d) and 4(e), respectively. We do observe an enhancement of 8% with an efficiency up to 86.20%, though the maximal efficiency is obtained at a bit longer optimal receiving time of 35.4

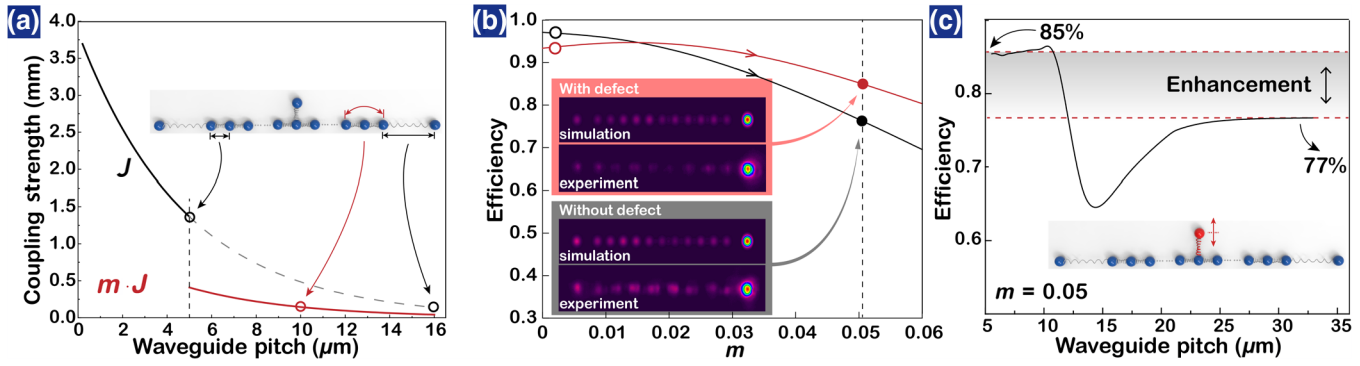

FIG. 5. Theoretical explanation of defect-induced efficiency enhancement. (a) The black line indicates the decay rate of coupling strength against pitch, and the red one shows the scenario where one waveguide is laid between them. m is the attenuation ratio of the coupling strength when a waveguide is laid in the middle. (b) Tuning m gradually, we find a long period where a defect enhances the transport process and the inset shows the comparison between experimental results and their modified simulation counterparts. (c) Taking m as 0.05, we simulate the transfer efficiency when the defect is moved close to and far away from the chain as shown in the inset. We mark the experimental results obtained with and without a defect on the simulated curve, and find that they are well consistent with our theoretical modeling.

mm. Hanbury-Brown-Twiss experiment also suggests a good preservation of quantum correlation with a measured anticorrelation up to 0.027 ± 0.0032.

In a general case, the nearest coupling is only considered [24] but in an experimental environment, our linear arrangement of waveguides has a very near pitch of 5 μm between each other, which means the next-nearest pitch is 10 μm and it is also non-negligible. Furthermore, we show that one waveguide laid in the middle will largely affect the propagation of evanescent wave. We therefore construct a modified model to explain the observed defect-induced enhancement of efficiency.

We consider that the coupling strength attenuates to m times ($0 < m < 1$) when a waveguide is laid in the middle. In consideration of the same propagation media, for the coupling coefficient J' plotted in red in Fig. 5(a), the exponential decay constant k of coupling strength against waveguide pitch p remains the same with that for J plotted in black in Fig. 5(a), i.e., $J = e^{-kp}$ and $J' = me^{-kp}$. The modified Hamiltonian H' is expanded as follows:

$$H' = H + \left(\sum_{i=2}^{N-3} mJ a_i^{\dagger} a_{i+2} + \text{c.c.} \right), \tag{5}$$

where H is the Hamiltonian in Eq. (1). We can find a continuously differential transfer efficiency [Fig. 5(b)] when the parameter m is adjusted dynamically from 0 to 0.06. With the m value of 0.05, we can obtain an increase of 8% from 77% (without defect) to 85% (with defect).

We may find that the defect can play a dual role in the model of photonic Newton's cradle. Ideally, the transfer efficiency should reach a unity. In practice, however, the defects introduced by fabrication or environment can induce a drop away from the expected value. Interestingly, we may also improve the transfer efficiency by the defect itself if we can artificially introduce the defect appropriate in light of a standard coupling mode theory.

III. CONCLUSION

In summary, we present an experimental demonstration of Newton's cradle by using a boundary-controlled chain on a photonic chip. Energy transport can be directly conducted between two remote sites with the same fashion of energy exchange and interaction mechanics in Newton's cradle. A long-range interaction is mediated by a long chain composed of 21 strongly coupled sites and a high retrieval efficiency can be obtained in both uniform and defect-doped chain structures. Our results may offer a new approach of flexible Hamiltonian engineering beyond geometric limitation, such as to bypass faulty nodes or to bridge remote terminals, enabling on-demand design and construction integrated quantum networks for quantum simulation.

ACKNOWLEDGMENTS

The authors thank Roberto Osellame, Chang-Pu Sun, and Jian-Wei Pan for helpful discussions. This work was supported by the National Key R&D Program of China (Grant No. 2017YFA0303700), the National Natural Science Foundation of China (Grants No. 61734005, No. 11761141014, and No. 11690033), the Science and Technology Commission of Shanghai Municipality (Grants No. 15QA1402200, No. 16JC1400405, and No. 17JC1400403), the Shanghai Municipal Education Commission (Grants No. 16SG09 and No. 2017-01-07-00-02-E00049), and the Zhiyuan Scholar Program (Grants No. ZIRC2016-01). X.-M.J. acknowledges support from the National Young 1000 Talents Plan. L.A.W. is supported by the Basque Government (Grant No. IT472-10) and the Spanish MINECO/FEDER, UE (Grant No. FIS2015-67161- P).

Z.F. and Z.-W.G. contributed equally to this work.

APPENDIX A: FABRICATION DETAILS

An ultrafast pulse focused into transparent materials can produce a permanent refractive index increase due to the localized nonlinear absorption process. A waveguide can be constructed with a translation of photonic wafer in three dimensions. The femtosecond laser (10 W, 1026 nm) with 290-fs pulse duration and 1-MHz repetition rate is frequency doubled to 513 nm, and is further fed into a spatial light modulator to create burst trains. By using a 50× objective lens with a numerical aperture of 0.55, we focus the laser on a borosilicate substrate (100 mm × 20 mm × 1 mm) to fabricate the chain structure consisting of 23 waveguides, each of which has an elliptical cross section about 7 μm × 5 μm.

APPENDIX B: COUPLING STRENGTH

The coupling strength between neighboring sites exponentially decreases with the site pitch as $J = 3.944 \times e^{-0.1899 \times p}$, where p is the site pitch in the unit of μm and the decay rate k equals 0.1899 in our borosilicate substrate. The strong coupling strength in the site train is about 1.526 mm^{-1} in the uniform site pitch of 5 μm among 21 nearest-neighbor sites. The boundary coupling strength is about 0.1890 mm^{-1} in the site pitch of 16 μm between the sending (or receiving) site and the nearest-neighboring site.

APPENDIX C: DETAILS OF SINGLE-PHOTON EXPERIMENT

A single photon at 810 nm, heralded from a spontaneous parametric down-conversion photon pair, is injected into the sending site in the photonic chip instead of classical light. Intensified CCD (ICCD) cameras with a gate width of 4.5 ns has a very good signal-to-noise ratio and single-photon sensitivity. The single-photon events can be

captured at the output end of the photonic chip [shown in Fig. 4(a)]. The other photon is delayed by a coiled optical fiber before registering at an avalanche photodiode D1. With the trigger from D1, we accumulate 3000 frames in 30 min to obtain the heralded single-photon results [shown in Fig. 4(c)]. Without the trigger, one arm of the photon pair is actually in a single-photon-level thermal state. The measured output intensity distribution is shown in Fig. 4(b).

We use a Hanbury-Brown-Twiss scheme to verify the ability of preserving the properties of single photons. By turning up the flipper mirror, photons can be collected into a fiber beam splitter. The two avalanche photodiodes D1 and D2 count photons at the two outputs of beam splitter and give the probability p_2 and p_3. Together with the probability p_1 obtained from D1, we can evaluate the intensity cross-correlation function by

$$g_{si} = \frac{(p_{12} + p_{13})}{p_1(p_2 + p_3)}. \tag{C1}$$

Besides, the anticorrelation $g^{(2)}(0)$ of heralded single photons ideally tends to zero and the mathematical expression is obtained in Eq. (4)

The cross correlation and anticorrelation are found to reach $g_{si} = 148.99 \pm 1.96$ and $g_H = 0.0089 \pm 0.0019$, respectively, which suggests a good preservation of quantum correlation.

[1] M. Bentivegna, N. Spagnolo, C. Vitelli, F. Flamini, N. Viggianiello, L. Latmiral, P. Mataloni, D. J. Brod, E. F. Galvão, A. Crespi, R. Ramponi, R. Osellame, and F. Sciarrino, Experimental scattershot Boson sampling, Sci. Adv. **1**, e1400255 (2015).

[2] I. Pitsios, L. Banchi, A. S. Rab, M. Bentivegna, D. Caprara, A. Crespi, N. Spagnolo, S. Bose, P. Mataloni, R. Osellame, and F. Sciarrino, Photonic simulation of entanglement growth and engineering after a spin chain quench, Nat. Commun. **8**, 1569 (2017).

[3] G. S. Engel, T. R. Calhoun, E. L. Read, T.-K. Ahn, T. Mančal, Y.-C. Cheng, R. E. Blankenship, and G. R. Fleming, Evidence for wavelike energy transfer through quantum coherence in photosynthetic systems, Nature **446**, 782 (2007).

[4] M. Mohseni, P. Rebentrost, S. Lloyd, and A. Aspuru-Guzik, Environment-assisted quantum walks in photosynthetic energy transfer, J. Chem. Phys. **129**, 174106 (2018).

[5] E. Rieper, J. Anders, and V. Vedral, Quantum entanglement between the electron clouds of nucleic acids in DNA, arXiv:1006.4053 (2010).

[6] M. Arndt, T. Juffmann, and V. Vedral, Quantum physics meets biology, HFSP J. **3**, 386 (2009).

[7] H. B. Perets, Y. Lahini, F. Pozzi, M. Sorel, R. Morandotti, and Y. Silberberg, Realization of Quantum Walks with Negligible Decoherence in Waveguide Lattices, Phys. Rev. Lett. **100**, 170506 (2008).

[8] T. Schwartz, G. Bartal, S. Fishman, and M. Segev, Transport and Anderson localization in disordered two-dimensional photonic lattices, Nature **446**, 52 (2007).

[9] Y. Lahini, A. Avidan, F. Pozzi, M. Sorel, R. Morandotti, D. N. Christodoulides, and Y. Silberberg, Anderson Localization and Nonlinearity in One-Dimensional Disordered Photonic Lattices, Phys. Rev. Lett. **100**, 013906 (2008).

[10] J. Maziero, L. C. Céleri, R. M. Serra, and V. Vedral, Classical and quantum correlations under decoherence, Phys. Rev. A **80**, 044102 (2009).

[11] Y. Yin, D. E. Katsanos, and S. N. Evangelou, Quantum walks on a random environment, Phys. Rev. A **77**, 022302 (2008).

[12] M. Christandl, N. Datta, A. Ekert, and A. J. Landahl, Perfect State Transfer in Quantum Spin Networks, Phys. Rev. Lett. **92**, 187902 (2004).

[13] M. Bellec, G. M. Nikolopoulos, and S. Tzortzakis, Faithful communication Hamiltonian in photonic lattices, Opt. Lett. **37**, 4504 (2012).

[14] R. J. Chapman, M. Santandrea, Z. Huang, G. Corrielli, A. Crespi, M.-H. Yung, R. Osellame, and A. Peruzzo, Experimental perfect state transfer of an entangled photonic qubit, Nat. Commun. **7**, 11339 (2016).

[15] A. Wójcik, T. Łuczak, P. Kurzyński, A. Grudka, T. Gdala, and M. Bednarska, Unmodulated spin chains as universal quantum wires, Phys. Rev. A **72**, 034303 (2005).

[16] N. Y. Yao, L. Jiang, A. V. Gorshkov, Z.-X. Gong, A. Zhai, L.-M. Duan, and M. D. Lukin, Robust Quantum State Transfer in Random Unpolarized Spin Chains, Phys. Rev. Lett. **106**, 040505 (2011).

[17] Z.-M. Wang, L.-A. Wu, M. Modugno, W. Yao, and B. Shao, Fault-tolerant almost exact state transmission, Sci. Rep. **3**, 3128 (2013).

[18] L.-A. Wu and D. A. Lidar, Power of anisotropic exchange interactions: Universality and efficient codes for quantum computing, Phys. Rev. A **65**, 042318 (2002).

[19] M. B. Plenio and F. L. Semião, High efficiency transfer of quantum information and multiparticle entanglement generation in translation-invariant quantum chains, New J. Phys. **7**, 73 (2005).

[20] T. Shi, Y. Li, Z. Song, and C.-P. Sun, Quantum-state transfer via the ferromagnetic chain in a spatially modulated field, Phys. Rev. A **71**, 032309 (2005).

[21] Y. Li, T. Shi, B. Chen, Z. Song, and C.-P. Sun, Quantum-state transmission via a spin ladder as a robust data bus, Phys. Rev. A **71**, 022301 (2005).

[22] L. Campos Venuti, C. Degli Esposti Boschi, and M. Roncaglia, Qubit Teleportation and Transfer across Antiferromagnetic Spin Chains, Phys. Rev. Lett. **99**, 060401 (2007).

[23] S. Oh, Y.-P. Shim, J. Fei, M. Friesen, and X. Hu, Effect of randomness on quantum data buses of Heisenberg spin chains, Phys. Rev. B **85**, 224418 (2012).

[24] J. Stolze, G. A. Alvarez, O. Osenda, and A. Zwick, *Quantum State Transfer and Network Engineering*, edited by G. M. Nikolopoulos and I. Jex (Springer, Berlin, Heidelberg, 2014), p. 149.

[25] J. Stolze and A. I. Zenchuk, Remote two-qubit state creation and its robustness, Quant. Inf. Process. **15**, 3347 (2016).

[26] R. Vieira and G. Rigolin, Almost perfect transport of an entangled two-qubit state through a spin chain, Phys. Lett. A **382**, 2586 (2018).
[27] A. Szameit, F. Dreisow, T. Pertsch, S. Nolte, and A. Tünnermann, Control of directional evanescent coupling in fs laser written waveguides, Opt. Express **15**, 1579 (2007).
[28] Z. Feng, B.-H. Wu, Y.-X. Zhao, J. Gao, L.-F. Qiao, A.-L. Yang, X.-F. Lin, and X.-M. Jin, Invisibility Cloak Printed on a Photonic Chip, Sci. Rep. **6**, 28527 (2016).
[29] H. Tang, C. Di Franco, Z.-Y. Shi, T.-S. He, Z. Feng, J. Gao, K. Sun, Z.-M. Li, Z.-Q. Jiao, T.-Y. Wang, M. S. Kim, and X.-M. Jin, Experimental quantum fast hitting on hexagonal graphs, Nat. Photonics **12**, 754 (2018).
[30] H. Tang, X.-F. Lin, Z. Feng, J.-Y. Chen, J. Gao, K. Sun, C.-Y. Wang, P.-C. Lai, X.-Y. Xu, Y. Wang, L.-F. Qiao, A.-L. Yang, and X.-M. Jin, Experimental two-dimensional quantum walk on a photonic chip, Sci. Adv. **4**, eaat3174 (2018).
[31] M. A. Nielsen and I. L. Chuang, Quantum computation and quantum information (Cambridge University Press, Cambridge, 2000).
[32] A. Zwick, G. A. Álvarez, J. Stolze, and O. Osenda, Quantum state transfer in disordered spin chains: How much engineering is reasonable? Quantum Inf. Comput. **15**, 582 (2015).
[33] J. B. Spring, P. S. Salter, B. J. Metcalf, P. C. Humphreys, M. Moore, N. Thomas-Peter, M. Barbieri, X.-M. Jin, N. K. Langford, W. S. Kolthammer, M. J. Booth, and I. A. Walmsley, On-chip low loss heralded source of pure single photons, Opt. Express **21**, 13522 (2013).
[34] M. B. Plenio and S. F. Huelga, Entangled Light from White Noise, Phys. Rev. Lett. **88**, 197901 (2002).
[35] F. Caruso, A. Crespi, A. G. Ciriolo, F. Sciarrino, and R. Osellame, Fast escape of a quantum walker from an integrated photonic maze, Nat. Commun. **7**, 11682 (2016).